

Tuning the anomalous Nernst and Hall effects with shifting the chemical potential in Fe-doped and Ni-doped $\text{Co}_3\text{Sn}_2\text{S}_2$

Jie Liu¹, Linchao Ding¹, Liangcai Xu¹, Xiaokang Li¹, Kamran Behnia², and Zengwei Zhu^{1,†}

¹Wuhan National High Magnetic Field Center and School of Physics,
Huazhong University of Science and Technology,
Wuhan, 430074, China

²Laboratoire de Physique et Etude des Matériaux (CNRS/UPMC),
Ecole Supérieure de Physique et de Chimie Industrielles,
10 Rue Vauquelin, 75005 Paris, France

(Dated: November 28, 2023)

$\text{Co}_3\text{Sn}_2\text{S}_2$ is believed to be a magnetic Weyl semimetal. It displays large anomalous Hall, Nernst and thermal Hall effects with a remarkably large anomalous Hall angle. Here, we present a comprehensive study of how substituting Co by Fe or Ni affects the electrical and thermoelectric transport. We find that doping alters the amplitude of the anomalous transverse coefficients. The maximum decrease in the amplitude of the low-temperature anomalous Hall conductivity σ_{ij}^A is twofold. Comparing our results with theoretical calculations of the Berry spectrum assuming a rigid shift of the Fermi level, we find that given the modest shift in the position of the chemical potential induced by doping, the experimentally observed variation occurs five times faster than expected. Doping affects the amplitude and the sign of the anomalous Nernst coefficient. Despite these drastic changes, the amplitude of the $\alpha_{ij}^A/\sigma_{ij}^A$ ratio at the Curie temperature remains close to $\approx 0.5k_B/e$, in agreement with the scaling relationship observed across many topological magnets.

I. INTRODUCTION

In magnetic Weyl semimetals, the linear band structure on the Fermi surface gives rise to a significant local fictitious magnetic field in momentum space known as Berry curvature which is associated with the topological properties of the Bloch waves of electrons in the host solid [1–3]. The absence of time inversion symmetry leads to a nonzero integral of the Berry curvature in momentum space. The anomalous Hall effect (AHE) can have both intrinsic and extrinsic origins [1]. In the intrinsic case, this effect is attributed to the Berry curvature. The extrinsic mechanism refers to either skew scattering or ‘side jump’ [1]. The anomalous Nernst effect (ANE) is a counterpart of the AHE. It emerges when mobile carriers respond to a temperature gradient [4–6].

The Mott relation [7] states that the thermoelectric conductivity is set by the energy derivative of the electric conductivity at the Fermi level. This relation can be used to give an account of the measured Nernst signal in different contexts [8]. A version of it is used to link the amplitude of the ordinary Nernst effect to the Hall mobility in metals [9]. Another version was invoked to give an account of a correlation observed between the amplitude of the anomalous Hall (σ_{ij}^A) and the anomalous Nernst (α_{ij}^A) conductivities across different topological magnets [10]. While the amplitude of each varies by orders of magnitude, their ratio at room temperature remains of the order of k_B/e [10].

The ANE is particularly sensitive to the band structure near Fermi level [3]. In 2D systems, the Fermi level can be tuned by varying the gate voltage. A sign reversal of ANE was revealed in the case of the magnetic topological insulator thin film $\text{Cr}_{0.15}(\text{Bi}_{0.1}\text{Sb}_{0.9})_{1.85}\text{Te}_3$ by tuning the

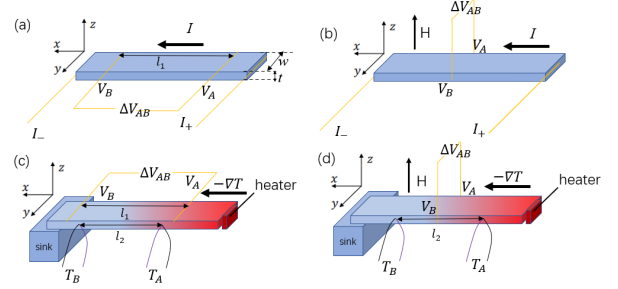


FIG. 1. The experimental setup for measuring (a) longitudinal resistivity, (b) Hall resistivity, (c) Seebeck coefficient and (d) Nernst coefficient, respectively. The formulas to obtain the transport coefficients can be found in the section II.

gate voltage [11]. In 3D systems, an effective approach to tune the Fermi level is chemical doping, which can significantly influence the amplitude of the ANE. A number of systems have been studied in this way, including $\text{Ga}_{1-x}\text{Mn}_x\text{As}$ dilute magnets [5], $\text{La}_{1-x}\text{Sr}_x\text{CoO}_3$ ferromagnetic oxides [12], as well as $\text{Co}_2\text{MnAl}_x\text{Si}_{1-x}$ magnetic Weyl metals [13].

The Shandite compound $\text{Co}_3\text{Sn}_2\text{S}_2$ is a magnetic Weyl semimetal with a remarkably large intrinsic anomalous Hall conductivity (AHC) (up to $1130 \Omega^{-1}\text{cm}^{-1}$) and anomalous Hall angle (up to 20% [14]). Its Curie temperature is 177 K and the magnetic moment corresponds to $0.29 \mu_B/\text{Co}$. Calculations and experiments indicated the presence of Weyl points located at 60 meV above the Fermi level [14–17]. This allows to adjust the topological property easily through doping [18–22] or by applying pressure [23–25]. The cobalt site can be doped by either nickel or iron. The tin site can be occupied by indium.

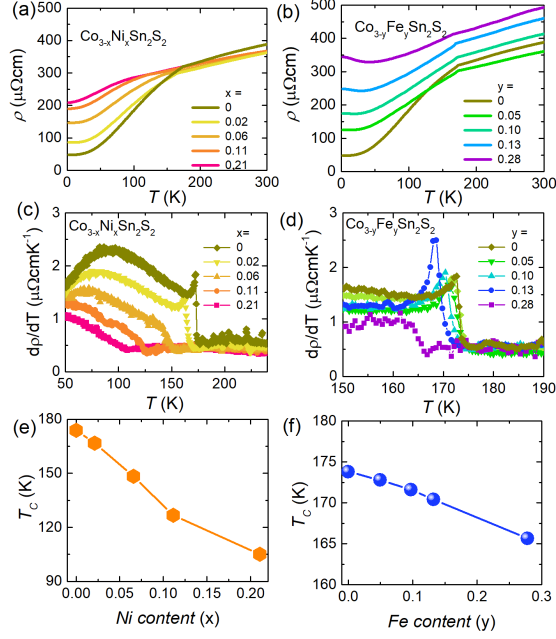


FIG. 2. (a) Temperature dependence of resistivity at zero-field of Ni doped $\text{Co}_3\text{Sn}_2\text{S}_2$ samples and (b) Fe doped samples. (c) Temperature dependence of the first derivative of resistivity for Ni doped $\text{Co}_3\text{Sn}_2\text{S}_2$ samples and (d) Fe doped samples. The evolution of Curie temperatures with doping ratio of (e) Ni content x and (f) Fe content y .

Upon chemical doping by iron, the AHC is further enhanced to $1850 \Omega^{-1}\text{cm}^{-1}$ and anomalous Hall angle up to 33% [18]. The elevations of AHC ($\sim 1400 \Omega^{-1}\text{cm}^{-1}$), AHA ($\sim 22\%$) in Ni-doped samples was attributed to the local disorder effect broadening the inverted bands [16], which remains intrinsic [21]. Indium doping enhances AHC [20] and introduces additional quantum phase transitions to the phase diagram [22, 26, 27]. A successful attempt in introducing electrons by replacing S with Sb has also been reported [28].

The anomalous Nernst effect in pristine $\text{Co}_3\text{Sn}_2\text{S}_2$ has been the subject of numerous studies [29–31]. By studying samples of different mobilities, Ding *et al.* [31] found that the ordinary (anomalous) Nernst effect (S_{yx}^O) increases (decreases) with increasing carrier mobility. This anti-correlation between ANE (S_{yx}^A) and carrier mobility was found to be in agreement with the intrinsic origin of the anomalous Nernst conductivity (α_{yx}^A) set by Berry curvature. On the theoretical side, calculations predict that In doping largely impacts the ANE [22].

Here, we present a systematic study of AHE and ANE in $\text{Co}_3\text{Sn}_2\text{S}_2$ samples doped with Fe or Ni. We find that the amplitude and the temperature dependence of AHE and ANE display a gradual evolution. The amplitude of the low-temperature Hall-conductivity σ_{ij}^A decreases by a factor of 2. The low-temperature anomalous Nernst effect changes sign. The variation of σ_{ij}^A with doping is much

more rapid than what is expected by theoretical expectations based on the quantification of the Berry spectrum [31] neglecting correlations and extrinsic contributions. Despite the notable variation in the temperature dependence of the Hall and Nernst conductivities, $\alpha_{ij}^A/\sigma_{ij}^A$ ratio barely changes at the Curie temperature. In doped samples, it displays an almost linear temperature dependence and becomes $\approx 0.5k_B/e$ near T_C , in agreement with the scaling relation found in other topological magnets [10].

II. METHODS

Electron doping is achieved by replacing Co with Ni and hole doping by substituting Co with Fe [32]. A stoichiometric ratio of Ni, Fe, Co, Sn and S powders was sealed in a quartz tube. We grew high quality single crystals of $\text{Co}_{3-x}\text{Ni}_x\text{Sn}_2\text{S}_2$ and $\text{Co}_{3-y}\text{Fe}_y\text{Sn}_2\text{S}_2$ by self-flux method as reported before [31, 33].

Shiny crystals were selected by careful mechanical separation after growth. Crystal stoichiometry was confirmed by energy dispersive X-ray spectroscopy (EDS) and the results are shown in Table I. Transport measurements were performed with a physical property measurement system (Quantum Design PPMS-9). A thermal or electrical current was applied along the a -axis [31]. Longitudinal and Hall resistivity were measured by a standard four-probe method. The Seebeck and the Nernst coefficients were measured using a chip-resistance heater and two pairs of thermocouples under high-vacuum environment of the PPMS. The schematic illustration of the experimental setup is shown in Fig. 1. We can obtain longitudinal resistivity, Hall resistivity, Seebeck coefficient and Nernst coefficient by $\rho_{xx} = \frac{\Delta V_{AB} w t}{I l_1}$, $\rho_{yx} = \frac{\Delta V_{AB} t}{I}$, $S_{xx} = \frac{E_x}{\nabla_x T} = -\frac{\Delta V_{AB}/l_1}{\Delta T_{AB}/l_2}$, $S_{yx} = \frac{E_y}{\nabla_x T} = -\frac{\Delta V_{AB}/w}{\Delta T_{AB}/l_2}$, respectively. Where $\Delta V_{AB} = V_A - V_B$, $\Delta T_{AB} = T_A - T_B$.

III. RESULTS AND DISCUSSION

Fig. 2(a) and 2(b) show the zero-field temperature-dependent resistivity of $\text{Co}_{3-x}\text{Ni}_x\text{Sn}_2\text{S}_2$ and $\text{Co}_{3-y}\text{Fe}_y\text{Sn}_2\text{S}_2$ samples. The Ni-substituted samples remain metallic with a residual resistivity, which

TABLE I. Elemental composition analysis results from the energy dispersive X-ray spectroscopy (EDS) for $\text{Co}_{3-x}\text{Ni}_x\text{Sn}_2\text{S}_2$ and $\text{Co}_{3-y}\text{Fe}_y\text{Sn}_2\text{S}_2$ single crystal samples with different doping ratios.

$\text{Co}_{3-x}\text{Ni}_x\text{Sn}_2\text{S}_2$					$\text{Co}_{3-y}\text{Fe}_y\text{Sn}_2\text{S}_2$				
x	Co	Ni	Sn	S	y	Co	Fe	Sn	S
0.02	2.98	0.02	2.07	1.92	0.05	2.95	0.05	2.09	1.91
0.06	2.94	0.06	2.11	1.91	0.10	2.90	0.10	2.08	1.90
0.11	2.89	0.11	2.09	1.93	0.13	2.87	0.13	2.09	1.90
0.21	2.79	0.21	2.10	1.87	0.28	2.72	0.28	2.05	1.87

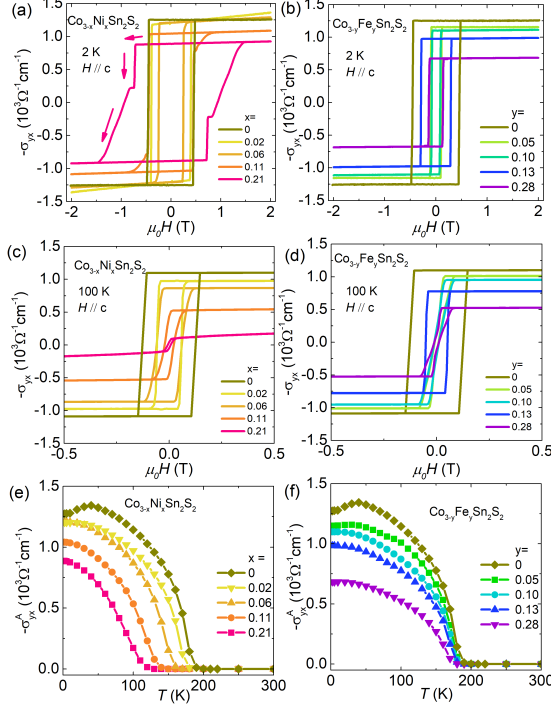


FIG. 3. (a). Field dependence of the Hall conductivity σ_{yx} of $\text{Co}_{3-x}\text{Ni}_x\text{Sn}_2\text{S}_2$ and (b). $\text{Co}_{3-y}\text{Fe}_y\text{Sn}_2\text{S}_2$ single crystal samples with different doping ratios at 2 K, respectively. (c). Field dependence of the Hall conductivity σ_{yx} of $\text{Co}_{3-x}\text{Ni}_x\text{Sn}_2\text{S}_2$ and (d). $\text{Co}_{3-y}\text{Fe}_y\text{Sn}_2\text{S}_2$ at 100 K. (e). Temperature dependence of anomalous Hall conductivity σ_{yx}^A of $\text{Co}_{3-x}\text{Ni}_x\text{Sn}_2\text{S}_2$ and (f). $\text{Co}_{3-y}\text{Fe}_y\text{Sn}_2\text{S}_2$.

increases with increasing x . In the case of Fe-substituted samples, the resistivity shows a low-temperature upturn when y exceeds 0.1 as reported previously and attributed to a Kondo effect [18]. Ordinarily, the Kondo effect completes with ferromagnetism [34]. However, the Kondo correlations can still be present, even ferromagnetism intends to suppress Kondo-assisted tunneling [34]. Several compounds has been proposed as the ferromagnetic Kondo system [35–37]. Interestingly, the Fe-doped samples with similar contents evolves earlier into the Kondo-like state. This may be due to the relative strong

TABLE II. Electron (hole) carrier density $[n(p)]$ (in units of 10^{19}cm^{-3}) together with their mobilities $[\mu_e(\mu_h)]$ (in units of $\text{cm}^2\text{V}^{-1}\text{s}^{-1}$) in different samples. They were extracted using a two-band fit of the ordinary Hall conductivity.

$\text{Co}_{3-x}\text{Ni}_x\text{Sn}_2\text{S}_2$						$\text{Co}_{3-y}\text{Fe}_y\text{Sn}_2\text{S}_2$				
x	0	0.02	0.06	0.11	0.21	y	0.05	0.10	0.13	0.28
p	8.45	8.24	7.78	7.14	6.73		10.20	11.72	13.11	15.14
n	8.46	9.93	10.60	12.81	15.12		8.12	7.83	7.18	6.34
μ_h	574	411	205	162	144		255	168	105	73
μ_e	465	431	234	160	127		285	216	163	135

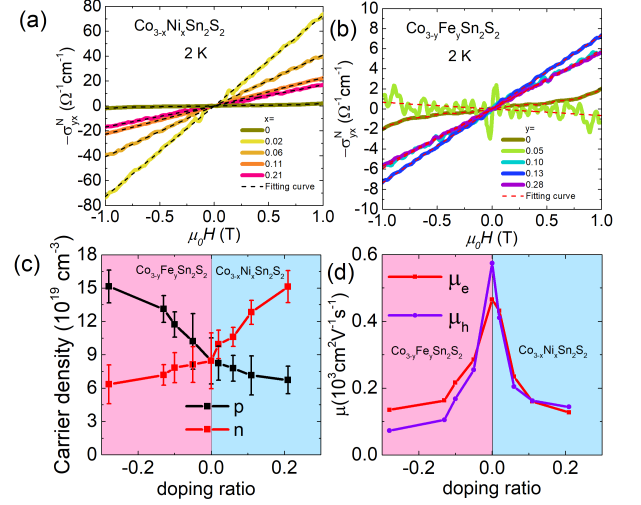


FIG. 4. (a). Low-field ordinary Hall conductivities of Ni doped $\text{Co}_{3-x}\text{Ni}_x\text{Sn}_2\text{S}_2$ samples and (b) Fe doped samples. Dashed lines are the fits with the two-band model. (c) The doping ratio dependence of carrier density. (d) Doping ratio dependence of mobilities obtained from the two-band model. The mobilities are reduced as dopants are increased.

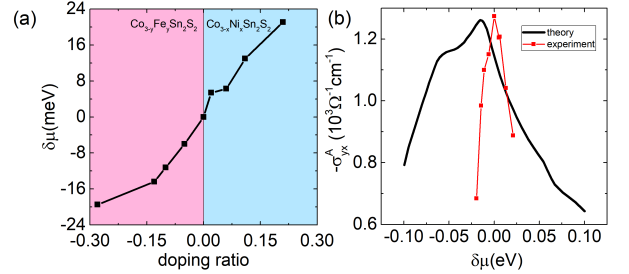


FIG. 5. (a) The doping ratio dependence of the shifted chemical potential. (b) The chemical potential dependence of the anomalous Hall conductivity. The black curve represents the result of theory[31] for the intrinsic contribution from Berry curvature, while the red curve is the experimental measured AHE result.

magnetism in iron. The coexist of ferromagnetism and Kondo effect would need to be further clarified. Since $k_f\ell = 44$ [33] when the residual resistivity is $200\ \mu\Omega\text{cm}$, one can exclude Anderson localization.

At Curie temperature, there is a visible kink in the temperature dependence of resistivity. In both Ni and Fe doped samples, this kink shifts to lower temperature with the increase in the dopant concentration. This is better illustrated in the temperature dependence of the first derivative of resistivity shown in Fig. 2(c) and Fig. 2(d). Fig. 2(e) and Fig. 2(f) show the evolution of the Curie temperature with doping contents, x and y . In $\text{Co}_{3-x}\text{Ni}_x\text{Sn}_2\text{S}_2$ samples, the Curie tempera-

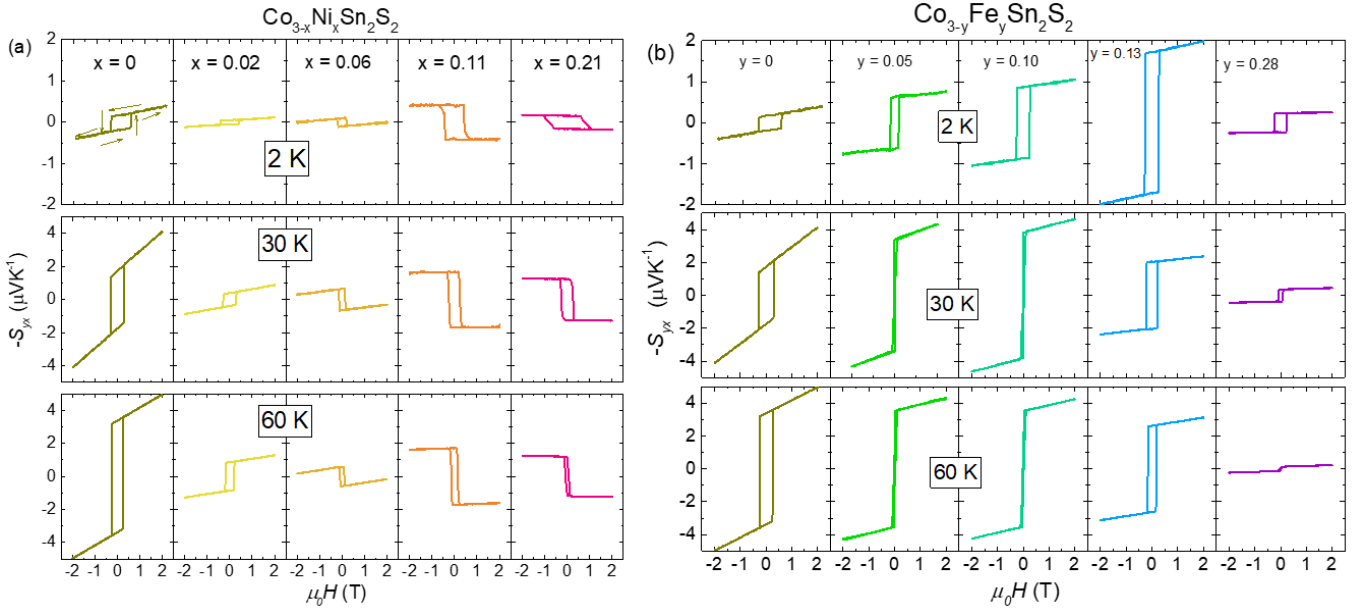


FIG. 6. (a) The field dependence of Nernst effect S_{yx} of $\text{Co}_{3-x}\text{Ni}_x\text{Sn}_2\text{S}_2$ and (b) $\text{Co}_{3-y}\text{Fe}_y\text{Sn}_2\text{S}_2$ at three typical temperatures: 2 K, 30 K and 60 K.

ture decreases with increasing x and the variation is very close to the results reported before [18, 21]. However, in $\text{Co}_{3-y}\text{Fe}_y\text{Sn}_2\text{S}_2$, a doping content of $y = 0.28$ pulls down the Curie temperature by less than 10 K. This is inconsistent with a previous report where the Curie temperature decreased by 25 K with a doping content of 0.2 [18]. The discrepancy is probably due to the different flux growth methods employed. Shen *et al.* [18] used Sn and Pb mixed flux to grow samples. On the other hand, our samples were grown by self-flux method. This calls for further studies for clarification.

The temperature dependence of Hall conductivity can be extracted from longitudinal resistivity ρ_{xx} and Hall resistivity ρ_{yx} , using $\sigma_{yx} = \frac{-\rho_{yx}}{\rho_{xx}^2 + \rho_{yx}^2}$. Fig. 3(a) and 3(b) present the magnetic field dependence of the Hall conductivity in $\text{Co}_{3-x}\text{Ni}_x\text{Sn}_2\text{S}_2$ and $\text{Co}_{3-y}\text{Fe}_y\text{Sn}_2\text{S}_2$ samples at 2 K with the field oriented along the c -axis. In $\text{Co}_{3-x}\text{Ni}_x\text{Sn}_2\text{S}_2$, the Hall conductivity shows an obvious hysteresis. The behavior changes as the doping increases. When the doping level is low, the jump in the Hall conductivity is very steep. After $x > 0.06$, the jump begins to widen. When the doping ratio is $x = 0.21$, the jump occurs in two steps along the direction indicated by the arrows in the figure.

A similar process was reported in ref. [16, 21]. The two-step jumps in the field dependence of the magnetization observed near the Curie temperature indicates mixed magnetic phases with magnetic moments oriented along in-plane and out-of-plane directions [16, 21]. When the magnetic field is swept, the inconsistency between the moment reversal process along in-plane and out-of-plane orientations leads to a two-step jump [38]. With the increase of doping ratio x , the mixed magnetic phases

survive down to low temperatures, indicating that Ni doping affects the magnetic structure. In contrast, Fe-doped samples display sharp jumps in the field dependence of their magnetization at low temperatures. Two-step jumps reappear when temperature becomes as high as 100 K. Both types of doping reduce the coercive field and the amplitude of the anomalous Hall signal, as shown in Fig. 3(c) and 3(d). The detailed magnetic structures of the doped samples is a subject for future experiments.

Fig. 3(e) and Fig. 3(f) show the temperature dependence of the AHC. With the increase of temperature, the magnetic moment tends to be disordered with the increase of thermal disturbance. Above the Curie temperature, the $\text{Co}_3\text{Sn}_2\text{S}_2$ is no more a magnetic Weyl semimetal, thus AHC tends to be 0 [18]. As seen in Fig. 3(e), AHC at 2 K decreases with the increase in the doping level in Ni-substituted samples. This is consistent with what was reported for Ni-substituted samples grown by self-flux method [21], but not with Ni-substituted samples grown by flux method by Shen *et al.* who found that AHC was enhanced to $1400 \Omega^{-1}\text{cm}^{-1}$ when $x=0.1$ [16]. The situation is similar in the case of Fe-substituted samples. As seen in Fig. 3(f), in $\text{Co}_{3-y}\text{Fe}_y\text{Sn}_2\text{S}_2$ grown by self-flux method, the 2 K AHC decreases monotonically with increasing y . In the Fe-substituted samples obtained by Shen *et al.* using the Sn and Pb flux method, AHC increased to $1800 \Omega^{-1}\text{cm}^{-1}$ when $y=0.05$ [18] in sharp contrast with what is observed here in samples obtained by the self-flux method here. This difference indicates that different growth methods influence the band structure and possibly the lattice constant.

We used a two-band model to fit the field dependence of the Hall conductivity and to quantify the evolution of

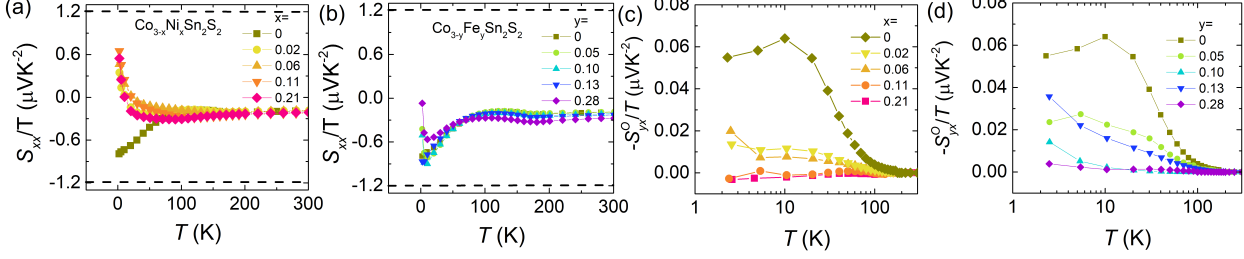


FIG. 7. (a) Temperature dependence of the Seebeck coefficient over temperature at zero-field of Ni doped $\text{Co}_3\text{Sn}_2\text{S}_2$ samples and (b) of Fe doped samples. (c). Temperature dependence of S_{yx}^O/T in samples with different doping ratios of $\text{Co}_{3-x}\text{Ni}_x\text{Sn}_2\text{S}_2$ and (d) $\text{Co}_{3-y}\text{Fe}_y\text{Sn}_2\text{S}_2$, respectively.

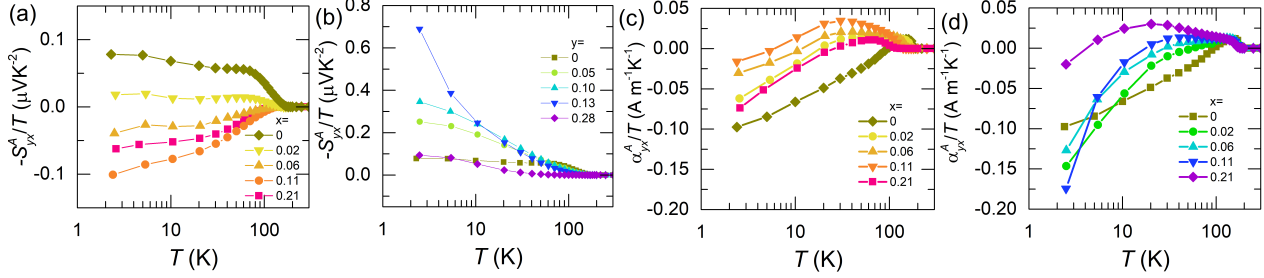


FIG. 8. (a). Temperature dependence of S_{yx}^A/T for $\text{Co}_{3-x}\text{Ni}_x\text{Sn}_2\text{S}_2$ and (b) $\text{Co}_{3-y}\text{Fe}_y\text{Sn}_2\text{S}_2$, respectively. (c) Temperature dependence of anomalous off-diagonal thermoelectric conductivity α_{yx}^A/T in $\text{Co}_{3-x}\text{Ni}_x\text{Sn}_2\text{S}_2$ and (d) $\text{Co}_{3-y}\text{Fe}_y\text{Sn}_2\text{S}_2$, respectively.

carrier density and mobility with doping. Fig. 4 (a) and (b) present fits to the extracted ordinary Hall conductivity at 2K, after subtracting the AHC component. For accuracy, the extracted parameters were checked with zero-field resistance. The parameters obtained from the fitting are listed in table II. Fig. 4 (c) displays the doping dependence of the carrier density of electrons (n) and holes (p). The electron carrier density (n) exceeds that of holes (p) in Ni-doped samples. In Fe-doped samples, the tendency is opposite. As expected, the carrier mobility decreases with both Co and Ni doping as shown in the Fig. 4 (d).

In order to compare with theory, we estimated the shift of the chemical potential induced by doping. It is shown in Fig. 5 (a). It was calculated using this equation:

$$\delta\mu = \frac{\hbar^2\pi^2(3\pi^2n_{ave})^{-1/3}}{2m^*}\delta n + \frac{\hbar^2\pi^2(3\pi^2n_{ave})^{-1/3}}{2m^*}\delta p \quad (1)$$

We took $m^*=0.65m_0$ [33], as effective mass, which is the average value obtained from quantum oscillations in the undoped sample. The average carrier density was taken to be: $n_{ave} = \frac{p+n}{2}$.

Neglecting any variation of the effective mass m^* with doping, one finds that the chemical potential varies from -19 meV to 20 meV for maximum p - and n -doping. Fig. 5 (b) compares the variation of the experimentally-

measured and theoretically computed AHC. They resemble qualitatively, but not quantitatively. There is a five-fold difference in the horizontal scale. Let us recall that there is also a twofold discrepancy between theoretically calculated and experimentally measured carrier density [33], presumably because theory neglects electron-electron interaction [33]. The fivefold discrepancy observed here may be partially due to a twofold mass renormalization due to interaction. Taken at its face value, it points to the existence of an extrinsic contribution with a sign of opposite to the intrinsic one.

Fig. 6 shows the field dependence of Nernst response for all doped samples at 2 K, 30 K and 60 K respectively. The Nernst signal consists of a slope (caused by the ordinary component) and a jump with hysteresis (caused by the anomalous components). In $\text{Co}_{3-x}\text{Ni}_x\text{Sn}_2\text{S}_2$, the sign of the anomalous Nernst signal S_{yx}^A changes from positive to negative between $x = 0.02$ to $x = 0.06$. In $\text{Co}_{3-y}\text{Fe}_y\text{Sn}_2\text{S}_2$, the ANE enhances with increasing y , and attains a maximum at $y = 0.13$. Afterwards, it decreases. The largest amplitude observed ($S_{yx}^A \approx -4\mu\text{V/K}$) was for a doping of $y = 0.10$ at 30 K.

Fig. 7 shows the temperature dependence of the Seebeck coefficient and the ordinary Nernst effect in all samples. S_{xx}/T for $\text{Co}_{3-x}\text{Ni}_x\text{Sn}_2\text{S}_2$ is shown in Fig. 7(a) and for $\text{Co}_{3-y}\text{Fe}_y\text{Sn}_2\text{S}_2$ in Fig. 7(b). In the pristine sample, S_{xx}/T is $\approx -0.2\mu\text{V/K}^2$ in most of the temperature range

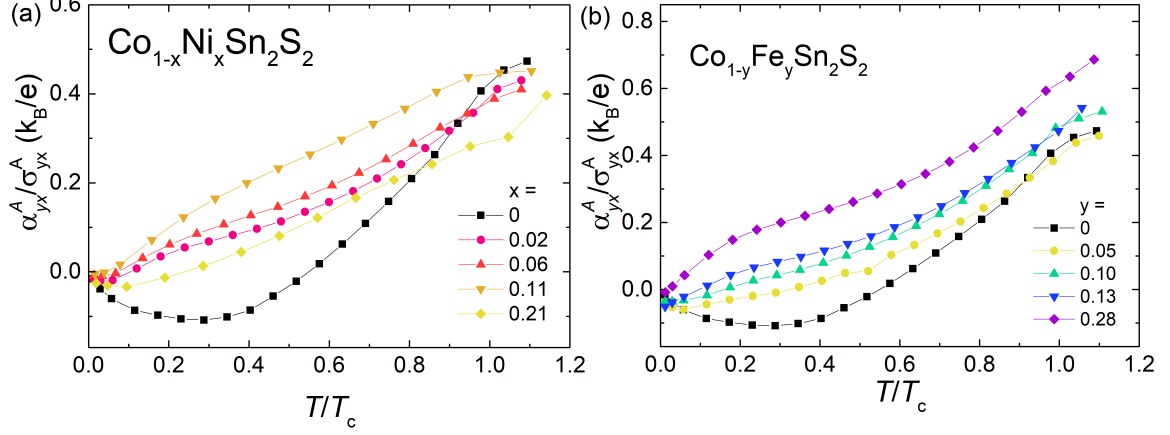


FIG. 9. (a) The temperature dependence of the ratio for $\alpha_{ij}^A/\sigma_{ij}^A$ of $\text{Co}_{3-x}\text{Ni}_x\text{Sn}_2\text{S}_2$ and (b) for $\text{Co}_{3-y}\text{Fe}_y\text{Sn}_2\text{S}_2$, respectively. The $\alpha_{ij}^A/\sigma_{ij}^A$ remains close to $\approx 0.5 k_B/e$ near the Curie temperature for all samples.

and then at below 100 K it tends towards $-0.8\mu\text{V}/\text{K}^2$. $\text{Co}_3\text{Sn}_2\text{S}_2$ is a compensated semi-metal with numerous small electron and hole pockets [33]. Because of the contributions of opposite signs, its overall Seebeck response should be smaller than what is expected S_{xx}/T from the Fermi temperature in a one-band picture [39]: $S_{xx}/T = \frac{\pi^2}{3} \frac{k_B}{e} \frac{k_B}{E_F} = |1.2| \mu\text{V}/\text{K}^2$. The average Fermi energy of a pocket can be estimated to be $\approx 20\text{meV}$ using $E_F = \frac{\pi^2 n_{\text{ave}} k_B^2}{2\gamma}$. Here $\gamma = 1.59 \text{ mJ}/(\text{molK}^2)$ [40] is the Sommerfeld coefficient and $n = 8.8 \times 10^{25} \text{ cm}^{-3}$ [31] is the carrier density. If the only carriers were electrons (holes), the expected S_{xx}/T would have been $-(+)|1.2\mu\text{V}/\text{K}^2$. In the perfectly compensated $\text{Co}_3\text{Sn}_2\text{S}_2$, S_{xx}/T should be somewhere between depending on the mobility of the hole-like and electron-like carriers. The fact that it is negative at low temperature indicates that the mean-free-path of occupied states is longer. In the Ni-doped samples (Fig. 7(a)) S_{xx}/T becomes positive below 20 K, which indicates that the mean-free-path of unoccupied states ('hole-like' carriers) becomes longer than the occupied states ('electron-like' carriers). In the case of Fe-doped samples, doping causes little change in S_{xx}/T , apart from a slight increase at temperatures. Note that the sign of the Seebeck coefficient depends on the competing contributions by occupied and unoccupied states. It is positive in copper, despite an electron-like Fermi surface, because unoccupied states contribute more than occupied states to the overall Seebeck response [8, 41].

The temperature dependence of the ordinary Nernst effect (ONE) extracted from our data is shown in Fig. 7 (c)-(d). As seen in Fig. 7 (c), in $\text{Co}_{3-x}\text{Ni}_x\text{Sn}_2\text{S}_2$, the ordinary Nernst coefficient S_{yx}^O/T decreases rapidly with doping, which is expected given the reduction in the mean free path [32]. At $x = 0.2$, ONE has a sign change. Fe doping also leads to a reduction in ONE, as

seen in Fig. 7(d). The comparison shows that ONE is less affected by Fe doping than by Ni doping.

Fig. 8 shows the ANE and the anomalous off-diagonal thermoelectric conductivity α_{yx}^A in all samples. As seen in Fig. 8(a), doping induces a complex evolution of the ANE. The sign of S_{yx}^A changes at all temperatures for $x > 0.06$. In Fig. 8 (b), one can see that compared to Ni doping, Fe doping has a larger impact on the low-temperature ANE. In addition, Fe doping also greatly enhances the anomalous Nernst coefficient in the low temperature region, up to six times.

The sign change of anomalous Nernst coefficient in Fig. 8(a) has been observed in $\text{Co}_{3-x}\text{Ni}_x\text{Sn}_2\text{S}_2$ as the doping ratio is increased, while the Nernst signal keeps its positive sign with Fe doping in the whole doping range. Such a change induced by the shift of Fermi level, is not accompanied with a sign change in AHC. In the dilute magnetic semiconductor material $\text{Ga}_{1-x}\text{Mn}_x\text{As}$, the anomalous Nernst coefficient changes sign with doping [5]. In the magnetic topological insulator thin film $\text{Cr}_{0.15}(\text{Bi}_{0.1}\text{Sb}_{0.9})_{1.85}\text{Te}_3$, the Fermi level can be tuned by the gate voltage V_g [11]. When $V_g > 100 \text{ V}$, the anomalous Nernst effect changes sign below 5K. Fig. 8(c) and Fig. 8(d) shows the temperature dependence of anomalous off-diagonal thermoelectric conductivity α_{yx}^A/T with temperature which is calculated from $\alpha_{yx}^A = S_{xx}\sigma_{yx}^A + S_{yx}\sigma_{xx}$ [31]. One can see that α_{yx}^A/T displays a large variation below the Curie temperature in both $\text{Co}_{3-x}\text{Ni}_x\text{Sn}_2\text{S}_2$ and $\text{Co}_{3-y}\text{Fe}_y\text{Sn}_2\text{S}_2$. α_{xy}^A is determined by the Berry curvature near the Fermi level. The energy band structure obtained by theoretical calculation shows that the Berry curvature exhibits dominantly negative value near the charge neutral point, which is caused by anticrossing bands [31]. Then large negative Berry curvature induces large negative α_{xy}^A/T at low temperature. Thus, the Berry curvature determines the sign change of

α_{xy}^A .

It is instructive to plot the α_{ij}^A and σ_{ij}^A ratio. Despite the complex evolution of both, this ratio does not show a strong variation at high temperature. As shown in the Fig. 9, the $\alpha_{yx}^A/\sigma_{yx}^A$ ratio remains close to $0.5 k_B/e$ near the Curie temperature and smoothly vanishes towards zero with decreasing temperature. It was already observed [10, 42], that the amplitude of $\alpha_{ij}^A/\sigma_{ij}^A$ in many topological magnetic materials is of the same order of magnitude. In the intrinsic picture, such a correlation arises because both quantities average the Berry curvature of the Fermi surface (but with pondering factors) [10, 31]. Our observation that the $\alpha_{yx}^A/\sigma_{yx}^A$ ratio barely changes by doping suggests that even in presence of a sizeable extrinsic contribution the $\alpha_{ij}^A/\sigma_{ij}^A$ ratio remains a sizable fraction of k_B/e near the ordering temperature.

IV. CONCLUSION

In summary, we studied the evolution of the anomalous Nernst and Hall conductivities in chemically doped $\text{Co}_3\text{Sn}_2\text{S}_2$ and found that the amplitude of the anomalous transverse electric and thermoelectric conductivities evolve with doping. The low-temperature anomalous Hall conductivity varies much more than what is ex-

pected according to the calculated Berry spectrum. This indicates that the extrinsic contributions matter. The anomalous Nernst effect displays a more complex evolution as a function of doping and temperature. Nevertheless, the amplitude and the temperature dependence of $\alpha_{ij}^A/\sigma_{ij}^A$ does not vary much with doping and remains close to $\approx 0.5 k_B/e$ near the Curie temperature.

V. ACKNOWLEDGMENTS

This work was supported by the National Science Foundation of China (Grant No.12004123, 51861135104 and No.11574097), the Fundamental Research Funds for the Central Universities (Grant no. 2019kfyXMBZ071) and the National Key Research and Development Program of China (Grant No.2022YFA1403503), K. B was supported by the Agence Nationale de la Recherche (ANR-19-CE30-0014-04) and the Weizmann-CNRS collaboration program. X. L. acknowledges the China National Postdoctoral Program for Innovative Talents (Grant No.BX20200143) and the China Postdoctoral Science Foundation (Grant No.2020M682386).

* zengwei.zhu@hust.edu.cn

-
- [1] N. Nagaosa, J. Sinova, S. Onoda, A. H. MacDonald, and N. P. Ong, Anomalous Hall effect, *Reviews of Modern Physics* **82**, 1539 (2010).
 - [2] D. Xiao, M.-C. Chang, and Q. Niu, Berry phase effects on electronic properties, *Reviews of Modern Physics* **82**, 1959 (2010).
 - [3] D. Xiao, Y. Yao, Z. Fang, and Q. Niu, Berry-phase effect in anomalous thermoelectric transport, *Physical Review Letters* **97**, 026603 (2006).
 - [4] S. Onoda, N. Sugimoto, and N. Nagaosa, Quantum transport theory of anomalous electric, thermoelectric, and thermal Hall effects in ferromagnets, *Phys. Rev. B* **77**, 165103 (2008).
 - [5] Y. Pu, D. Chiba, F. Matsukura, H. Ohno, and J. Shi, Mott relation for anomalous Hall and Nernst effects in $\text{Ga}_{1-x}\text{Mn}_x\text{As}$ ferromagnetic semiconductors, *Physical Review Letters* **101**, 117208 (2008).
 - [6] X. Li, L. Xu, L. Ding, J. Wang, M. Shen, X. Lu, Z. Zhu, and K. Behnia, Anomalous Nernst and Righi-Leduc effects in Mn_3Sn : Berry curvature and entropy flow, *Physical Review Letters* **119**, 056601 (2017).
 - [7] N. F. Mott and E. A. Davis, *Electronic Processes in Non-Crystalline Materials* (Clarendon, Oxford, 1971).
 - [8] K. Behnia, *Fundamentals of Thermoelectricity* (Oxford University Press, 2015).
 - [9] K. Behnia and H. Aubin, Nernst effect in metals and superconductors: a review of concepts and experiments, *Rep. Prog. Phys.* **79**, 046502 (2016).
 - [10] L. Xu, X. Li, L. Ding, T. Chen, A. Sakai, B. Fauqué, S. Nakatsuji, Z. Zhu, and K. Behnia, Anomalous transverse response of Co_2MnGa and universality of the room-temperature $\alpha_{ij}^A/\sigma_{ij}^A$ ratio across topological magnets, *Physical Review B* **101**, 180404 (2020).
 - [11] M. Guo, Y. Ou, Y. Xu, Y. Feng, G. Jiang, K. He, X. Ma, Q.-K. Xue, and Y. Wang, Ambi-polar anomalous Nernst effect in a magnetic topological insulator, *New Journal of Physics* **19**, 113009 (2017).
 - [12] T. Miyasato, N. Abe, T. Fujii, A. Asamitsu, S. Onoda, Y. Onose, N. Nagaosa, and Y. Tokura, Crossover behavior of the anomalous Hall effect and anomalous Nernst effect in itinerant ferromagnets, *Physical Review Letters* **99**, 086602 (2007).
 - [13] A. T. Breidenbach, H. Yu, T. A. Peterson, A. P. McFadden, W. K. Peria, C. J. Palmström, and P. A. Crowell, Anomalous Nernst and Seebeck coefficients in epitaxial thin film $\text{Co}_2\text{MnAl}_x\text{Si}_{1-x}$ and Co_2FeAl , *Phys. Rev. B* **105**, 144405 (2022).
 - [14] E. Liu, Y. Sun, N. Kumar, L. Muechler, A. Sun, L. Jiao, S.-Y. Yang, D. Liu, A. Liang, Q. Xu, J. Kroder, V. Süß, H. Borrmann, C. Shekhar, Z. Wang, C. Xi, W. Wang, W. Schnelle, S. Wirth, Y. Chen, S. T. B. Goennenwein, and C. Felser, Giant anomalous Hall effect in a ferromagnetic kagome-lattice semimetal, *Nature Physics* **14**, 1125 (2018).
 - [15] Q. Wang, Y. Xu, R. Lou, Z. Liu, M. Li, Y. Huang, D. Shen, H. Weng, S. Wang, and H. Lei, Large intrinsic anomalous Hall effect in half-metallic ferromagnet $\text{Co}_3\text{Sn}_2\text{S}_2$ with magnetic Weyl fermions, *Nature Communications* **9**, 3681 (2018).
 - [16] J. Shen, Q. Yao, Q. Zeng, H. Sun, X. Xi, G. Wu, W. Wang, B. Shen, Q. Liu, and E. Liu, Local disorder-induced elevation of intrinsic anomalous Hall conduc-

- tance in an electron-doped magnetic Weyl semimetal, *Physical Review Letters* **125**, 086602 (2020).
- [17] L. Muechler, E. Liu, J. Gayles, Q. Xu, C. Felser, and Y. Sun, Emerging chiral edge states from the confinement of a magnetic Weyl semimetal in $\text{Co}_3\text{Sn}_2\text{S}_2$, *Physical Review B* **101**, 115106 (2020).
- [18] J. Shen, Q. Zeng, S. Zhang, H. Sun, Q. Yao, X. Xi, W. Wang, G. Wu, B. Shen, Q. Liu, and E. Liu, 33% giant anomalous Hall current driven by both intrinsic and extrinsic contributions in magnetic Weyl semimetal $\text{Co}_3\text{Sn}_2\text{S}_2$, *Advanced Functional Materials* **30**, 2000830 (2020).
- [19] J. Corps, P. Vaqueiro, A. Aziz, R. Grau-Crespo, W. Kockelmann, J.-C. Jumas, and A. V. Powell, Interplay of metal-atom ordering, fermi level tuning, and thermoelectric properties in cobalt shandites $\text{Co}_3\text{M}_2\text{S}_2$ ($\text{M} = \text{Sn, In}$), *Chemistry of Materials* **27**, 3946 (2015).
- [20] H. Zhou, G. Chang, G. Wang, X. Gui, X. Xu, J.-X. Yin, Z. Guguchia, S. S. Zhang, T.-R. Chang, H. Lin, W. Xie, M. Z. Hasan, and S. Jia, Enhanced anomalous Hall effect in the magnetic topological semimetal $\text{Co}_3\text{Sn}_{2-x}\text{In}_x\text{S}_2$, *Physical Review B* **101**, 125121 (2020).
- [21] G. S. Thakur, P. Vir, S. N. Guin, C. Shekhar, R. Wehrich, Y. Sun, N. Kumar, and C. Felser, Intrinsic anomalous Hall effect in Ni-substituted magnetic Weyl semimetal $\text{Co}_3\text{Sn}_2\text{S}_2$, *Chemistry of Materials* **32**, 1612 (2020).
- [22] Y. Yanagi, J. Ikeda, K. Fujiwara, K. Nomura, A. Tsukazaki, and M.-T. Suzuki, First-principles investigation of magnetic and transport properties in hole-doped shandite compounds $\text{Co}_3\text{In}_x\text{Sn}_{2-x}\text{S}_2$, *Physical Review B* **103**, 205112 (2021).
- [23] X. Chen, M. Wang, C. Gu, S. Wang, Y. Zhou, C. An, Y. Zhou, B. Zhang, C. Chen, Y. Yuan, M. Qi, L. Zhang, H. Zhou, J. Zhou, Y. Yao, and Z. Yang, Pressure-tunable large anomalous Hall effect of the ferromagnetic kagome-lattice Weyl semimetal $\text{Co}_3\text{Sn}_2\text{S}_2$, *Phys. Rev. B* **100**, 165145 (2019).
- [24] Z. Y. Liu, T. Zhang, S. X. Xu, P. T. Yang, Q. Wang, H. C. Lei, Y. Sui, Y. Uwatoko, B. S. Wang, H. M. Weng, J. P. Sun, and J.-G. Cheng, Pressure effect on the anomalous Hall effect of ferromagnetic Weyl semimetal $\text{Co}_3\text{Sn}_2\text{S}_2$, *Phys. Rev. Materials* **4**, 044203 (2020).
- [25] Q. Zeng, H. Sun, J. Shen, Q. Yao, Q. Zhang, N. Li, L. Jiao, H. Wei, C. Felser, Y. Wang, Q. Liu, and E. Liu, Pressure-driven magneto-topological phase transition in a magnetic Weyl semimetal, *Advanced Quantum Technologies* **5**, 2100149 (2022).
- [26] Z. Guguchia, H. Zhou, C. N. Wang, J. X. Yin, C. Mielke, S. S. Tsirkin, I. Belopolski, S. S. Zhang, T. A. Cochran, T. Neupert, R. Khasanov, A. Amato, S. Jia, M. Z. Hasan, and H. Luetkens, Multiple quantum phase transitions of different nature in the topological kagome magnet $\text{Co}_3\text{Sn}_{2-x}\text{In}_x\text{S}_2$, *npj Quantum Materials* **6**, 50 (2021).
- [27] M. Fujioka, T. Shibuya, J. Nakai, K. Yoshiyasu, Y. Sakai, Y. Takano, Y. Kamihara, and M. Matoba, The effect of simultaneous substitution on the electronic band structure and thermoelectric properties of Se-doped $\text{Co}_3\text{SnInS}_2$ with the kagome lattice, *Solid State Communications* **199**, 56 (2014).
- [28] Y. Li, W. Li, J. Lin, Z. Guo, F. Sun, X. Chen, Y. Luo, J. Yang, and W. Yuan, Electron doping and physical properties in the ferromagnetic semimetal $\text{Co}_3\text{Sn}_{2-x}\text{Sb}_x\text{S}_2$, *The Journal of Physical Chemistry C* **126**, 7230 (2022).
- [29] H. Yang, W. You, J. Wang, J. Huang, C. Xi, X. Xu, C. Cao, M. Tian, Z.-A. Xu, J. Dai, and Y. Li, Giant anomalous Nernst effect in the magnetic Weyl semimetal $\text{Co}_3\text{Sn}_2\text{S}_2$, *Phys. Rev. Mater.* **4**, 024202 (2020).
- [30] S. N. Guin, P. Vir, Y. Zhang, N. Kumar, S. J. Watzman, C. Fu, E. Liu, K. Manna, W. Schnelle, J. Gooth, C. Shekhar, Y. Sun, and C. Felser, Zero-field Nernst effect in a ferromagnetic kagome-lattice Weyl-semimetal $\text{Co}_3\text{Sn}_2\text{S}_2$, *Advanced Materials* **31**, 1806622 (2019).
- [31] L. Ding, J. Koo, L. Xu, X. Li, X. Lu, L. Zhao, Q. Wang, Q. Yin, H. Lei, B. Yan, Z. Zhu, and K. Behnia, Intrinsic anomalous Nernst effect amplified by disorder in a half-metallic semimetal, *Phys. Rev. X* **9**, 041061 (2019).
- [32] M. A. Kassem, Y. Tabata, T. Waki, and H. Nakamura, Structure and magnetic properties of flux grown single crystals of $\text{Co}_{3-x}\text{Fe}_x\text{Sn}_2\text{S}_2$ shandites, *Journal of Solid State Chemistry* **233**, 8 (2016).
- [33] L. Ding, J. Koo, C. Yi, L. Xu, H. Zuo, M. Yang, Y. Shi, B. Yan, K. Behnia, and Z. Zhu, Quantum oscillations, magnetic breakdown and thermal Hall effect in $\text{Co}_3\text{Sn}_2\text{S}_2$, *Journal of Physics D: Applied Physics* **54**, 454003 (2021).
- [34] A. N. Pasupathy, R. C. Bialczak, J. Martinek, J. E. Grose, L. A. K. Donev, P. L. McEuen, and D. C. Ralph, The Kondo effect in the presence of ferromagnetism, *Science* **306**, 86 (2004).
- [35] C. Krellner, N. S. Kini, E. M. Brünig, K. Koch, H. Rosner, M. Nicklas, M. Baenitz, and C. Geibel, CeRuPO : A rare example of a ferromagnetic Kondo lattice, *Physical Review B* **76**, 104418 (2007).
- [36] A. Tursina, E. Khamitcaeva, D. Gnida, and D. Kaczorowski, CePd_2Al_8 – a ferromagnetic Kondo lattice with new type of crystal structure, *Journal of Alloys and Compounds* **731**, 229 (2018).
- [37] D. Das and D. Kaczorowski, Ferromagnetic Kondo lattice behavior in $\text{Ce}_{11}\text{Pd}_4\text{In}_9$, *Journal of Magnetism and Magnetic Materials* **471**, 315 (2019).
- [38] M. A. Kassem, Y. Tabata, T. Waki, and H. Nakamura, Unconventional critical behaviors at the magnetic phase transition of $\text{Co}_3\text{Sn}_2\text{S}_2$ kagomé ferromagnet, *Journal of Physics: Condensed Matter* **33**, 015801 (2020).
- [39] K. Behnia, D. Jaccard, and J. Flouquet, On the thermoelectricity of correlated electrons in the zero-temperature limit, *Journal of Physics: Condensed Matter* **16**, 5187 (2004).
- [40] J. Hu, X. Kan, Z. Chen, G. Zheng, and Y. Ma, The magnetic, thermal transport properties, magnetothermal effect and critical behavior of $\text{Co}_3\text{Sn}_2\text{S}_2$ single crystal, *Journal of the American Ceramic Society* **105**, 4827 (2022).
- [41] J. E. Robinson, Thermoelectric power in the nearly-free-electron model, *Phys. Rev.* **161**, 533 (1967).
- [42] T. Asaba, V. Ivanov, S. M. Thomas, S. Y. Savrasov, J. D. Thompson, E. D. Bauer, and F. Ronning, Colossal anomalous Nernst effect in a correlated noncentrosymmetric kagome ferromagnet, *Science Advances* **7**, eabf1467 (2021).